



Contents lists available at ScienceDirect

Journal of Neuroscience Methods

journal homepage: www.elsevier.com/locate/jneumeth

Indirect relation based individual metabolic network for identification of mild cognitive impairment



Ying Li^{a,b}, Zhijun Yao^c, Huaxiang Zhang^a, Bin Hu^{a,c,*},¹, for the Alzheimer's Disease Neuroimaging Initiative²

^a School of Information Science and Engineering, Shandong Normal University, Jinan, China

^b Key Laboratory of TCM Data Cloud Service in Universities of Shandong, Shandong Management University, Jinan, China

^c Key Laboratory of Wearable Computing of Gansu Province, Lanzhou University, Lanzhou, China

ARTICLE INFO

Keywords:

Individual metabolic network
Indirect relation
Lattice-Close-Degree
Mild cognitive impairment (MCI)
FDG-PET

ABSTRACT

Background: Optimized abnormalities of individual brain network may allow earlier detection of mild cognitive impairment (MCI) and accurate prediction of its conversion to Alzheimer's disease (AD). Currently, most studies constructed individual networks based on region-to-region correlation without employing multi-region information. In order to develop the potential discriminative power of network and provide supportive evidence for feasibility of individual metabolic network study, we propose a new approach to extract features from network with indirect relation based on ¹⁸F-FDG PET data.

New Method: Direct relation based individual network is first constructed using Gaussian kernel function. After that, the lattice-close-degree in fuzzy mathematics is applied to reflect region-to-region indirect relation using the direct relations of regions and their common neighbors. The proposed approach has been evaluated on 199 MCI subjects and 166 normal controls (NC) using SVM classifier.

Results: The indirect relation based network features significantly promote classification performance in separating MCI from normal controls (NC) as well as MCI converters from non-converters. Specially, further improvements can be obtained by combining indirect relation features with ADAS-cog scores. Moreover, the discriminative regions we found are consistent with previous studies, indicating the efficacy of our constructed network in identifying correct biomarkers for diagnosing MCI and predicting its conversion.

Comparison with Existing Method(s): More accurate MCI identification of PET data can be achieved by features of network with indirect relation.

Conclusions: This work provides a new way to investigate brain network from metabolic perspective for accurate identification of MCI.

1. Introduction

Alzheimer's disease (AD) is a progressive, irreversible neurodegenerative disease accompanied by structural and functional changes in the brain (Dartigues, 2009; Mayeux and Stern, 2012; Prince et al., 2015). As the most prevalent form of dementia, AD is characterized by the decline of cognitive and memory functions, and it interferes people's daily life seriously (Reisberg et al., 1982; Smith et al., 1997; Brookmeyer et al., 1998). Mild cognitive impairment (MCI), commonly

characterized by slight cognitive deficits but largely intact activities of daily living is a transitional stage between the healthy aging and dementia (Petersen, 2004). Individuals with MCI tend to progress to AD at a rate of approximately 10–15% per year (Hänninen et al., 2000; Grundman et al., 2004) while normal controls (NC) develop dementia at a lower rate of 1–2% per year (Bischkopf et al., 2002). Thus, diagnose MCI especially progress MCI as early as possible is of great clinical importance to potentially delay and prevent transition from MCI to AD.

The human brain is a complicated network whose interregional

* Corresponding author at: School of Information Science and Engineering, Shandong Normal University, No. 1, University Road, Science Park, Jinan, Shandong, 250358, China.

E-mail address: bh@lzu.edu.cn (B. Hu).

¹ Key Laboratory of Wearable Computing of Gansu Province, Lanzhou University, No. 222 Tianshui Road, Lanzhou, Gansu, 730000, China.

² Data used in preparation of this article were obtained from the Alzheimer's Disease Neuroimaging Initiative (ADNI) database (adni.loni.usc.edu). As such, the investigators within the ADNI contributed to the design and implementation of ADNI and/or provided data but did not participate in analysis or writing of this report. A complete listing of ADNI investigators can be found at: http://adni.loni.usc.edu/wp-content/uploads/how_to_apply/ADNI_Acknowledgement_List.pdf.

<https://doi.org/10.1016/j.jneumeth.2018.09.007>

Received 13 March 2018; Received in revised form 5 July 2018; Accepted 3 September 2018

Available online 05 September 2018

0165-0270/ © 2018 Elsevier B.V. All rights reserved.

interactions enable the efficient processing of information and thus support complex brain functions (Park and Friston, 2013). Plenty of studies suggested that pathological attacks, including AD, bring significant alterations to the anatomical and functional brain structures (Wee et al., 2013). Specifically, AD-associated abnormalities involve not only the functional connection of several specific encephalic regions such as the hippocampus (Celone et al., 2006; Yousofzadeh et al., 2017), cingulate (Frisoni et al., 2010; Hafkemeijer et al., 2015; Yu et al., 2015), and precuneus (Langbaum et al., 2009; Camus et al., 2012; Rathore et al., 2017), but also the functional integration of the entire brain network (Stam et al., 2006; Illan et al., 2011). Therefore, the network representation is beneficial for researchers to obtain exclusive information reflecting an important aspect of the associations and interactions between multiple regions, which is not evident in local structure information. Thus far, many efforts have been made to construct networks for the purpose of AD and MCI detection using data of different neuroimaging techniques, such as structural magnetic resonance imaging (MRI) (Prasad et al., 2015; Beheshti et al., 2017), diffusion tensor imaging (DTI) (Wee et al., 2011; Shao et al., 2012), functional MRI (fMRI) (Chen et al., 2011; Jie et al., 2014a, 2014b; Wang et al., 2015; Khazaee et al., 2016), positron emission tomography (PET) (Yao et al., 2015, 2017). Some researchers constructed one network with a large population (He et al., 2007a, 2007b; Yao et al., 2015; Liu et al., 2017). For instance, He et al. (2007a) constructed network using Pearson correlation coefficient by cortical thickness and revealed the robust small-world properties of the network. Liu et al. (2017) extracted brain networks from AD and NC groups via independent component analysis (ICA) and constructed Cox models to identify risk factors for MCI group using MRI and PET data. Although these contribute to investigate the brain differences in group-level, they limit the application on the investigation of individual variability, particularly in identifying brain abnormalities in single patients. To deal with this, studies such as (Raj et al., 2010; Wee et al., 2011; Zhou et al., 2011; Dai et al., 2012; Li et al., 2012; Wee et al., 2013; Zheng et al., 2015; Hee-Jong et al., 2016; Yao et al., 2017) established network for each subject, namely individual network. Dai et al. (2012) and Wee et al. (2013) have employed similar methods that construct individual thickness network via region-to-region distances and exponential function. Zheng et al. (2015) proposed a multi-distance combination to evaluate between-region dissimilarity and transform the dissimilarity to connectivity via inverse-proportional function. Yao et al. (2017) constructed the individual metabolic network using cubes which were composed of certain numbers of voxels.

However, these studies of individual network construction compute region-to-region correlation only using limited information of two regions, ignore the fact that the relations of regions and their common neighbors could reflect two regions' correlation comprehensively, which may provide more deep inherent information. In addition, PET is a standardized non-invasive, three-dimensional functional imaging modality measuring the brain's rate of glucose metabolism (Nordberg et al., 2010). In AD and MCI, characteristic brain regions show decreased glucose metabolism, specifically in temporoparietal association cortices, posterior cingulate and precuneus, as well as frontal cortex and whole brain in more severely affected patients (Herholz, 2003, 2010; Illan et al., 2011; Chen et al., 2016). In view of the structural and functional connections in the brain, the glucose metabolism rate of different brain areas have some correlations, whose changes could reflect the dementia severity. In present study, we propose to construct indirect relation based individual metabolic network using [^{18}F] Fluorodeoxyglucose PET (^{18}F -FDG PET) data, which provides a new family of features for accuracy identification of MCI. Firstly, we construct direct relation based individual brain network. Euclidean distance is employed to reflect region-to-region dissimilarity, and then the dissimilarity is transformed into correlation by exponential function. Secondly, indirect relation based individual brain network is constructed. The relations of two regions and their common neighbors

compose of two fuzzy sets, respectively. The lattice-close-degree in fuzzy mathematics is applied to reflect the correlation of the two fuzzy sets, namely, the indirect relation of two regions. The performance of the proposed network is evaluated by SVM classifier. Results show that the indirect relation based network features can significantly improve MCI detection performance when compare with direct relation features. Furthermore, the indirect relation network is combined with cognitive measures to gain further promotion. Finally, a weight-based statistics method is utilized to find the most discriminative regions, whose results are consistent with previous literatures. To our knowledge, there's few attention paid to the construction of indirect relation based individual metabolic network, our method provides supportive evidence for the effectiveness of metabolic network in MCI identification, and further exploration is needed within such domain.

The remainder of the paper is structured as follows: Section 2 describes the material and methods in detail, which includes data acquisition from ADNI database, construction of individual network, feature reduction, and classification; and then the experimental results are presented, followed by a discussion which summarizes our findings, limitations and future directions.

2. Material and methods

2.1. Data acquisition

Data used in this study were obtained from the Alzheimer's disease Neuroimaging Initiative (ADNI) database (<http://www.loni.ucla.edu/ADNI/>). Supported by public-private partnership, the ADNI was launched in 2003. It is an ongoing and comprehensive project whose goal is to detect Alzheimer's disease at the earliest stage possible and develop ways to track the disease through biomarkers. The ADNI includes biospecimens, genetic, neuroimaging and clinical data collected from more than 50 research sites. Baseline FDG-PET data from 365 ADNI participants were used in this study. These subjects include (i) NC subjects, if diagnosis was normal at baseline; (ii) Stable MCI (sMCI) subjects, if diagnosis was MCI at baseline and not converted to AD after baseline within 36 months; (iii) Progressive MCI (pMCI) subjects, if diagnosis was MCI at baseline but these subjects converted to AD after baseline within 36 months. The demographic information and statistics of clinical assessments of the subjects are illustrated in Table 1.

FDG-PET scans were acquired according to a standardized protocol. Subjects to be imaged were asked to omit all food and fluids (except water) for at least 4 h prior to the imaging session. In imaging center, subjects lay quietly with eyes open in a room where the ambient noise is minimal and the light is standardized. After being injected with 5 ± 0.5 mCi (185 MBq) of [^{18}F]-FDG, subjects were allowed to rest comfortably for 20 min for the incorporation of [^{18}F]-FDG into the brain. Finally, a dynamic 3D scan consisting of six five-minute frames was acquired. For the FDG-PET data, subsequent preprocessing steps are as follows. Firstly, separate frames were co-registered to the first extracted frame of the raw image file to lessen the effects of patient motion. Secondly, average the co-registered frames to create a single image. Thirdly, the co-registered and averaged images were reoriented into a standard image grid, having 1.5 mm cubic voxels. Finally, the above-mentioned images were smoothed by a scanner-specific filter function to produce images of a uniform isotropic resolution of 8 mm

Table 1
Demographic and clinical information of the subjects.

Variables	NC	sMCI	pMCI
No. of subjects(Male/Female)	166(83/83)	96(56/40)	103(60/43)
Age(mean \pm SD)	74.36 \pm 5.08	73.98 \pm 7.30	73.71 \pm 7.06
CDR	0	0.5	0.5
MMSE score(mean \pm SD)	28.99 \pm 1.21	27.72 \pm 1.54	26.96 \pm 1.67
ADAS-cog score(mean \pm SD)	9.78 \pm 4.20	14.12 \pm 5.38	21.06 \pm 5.54

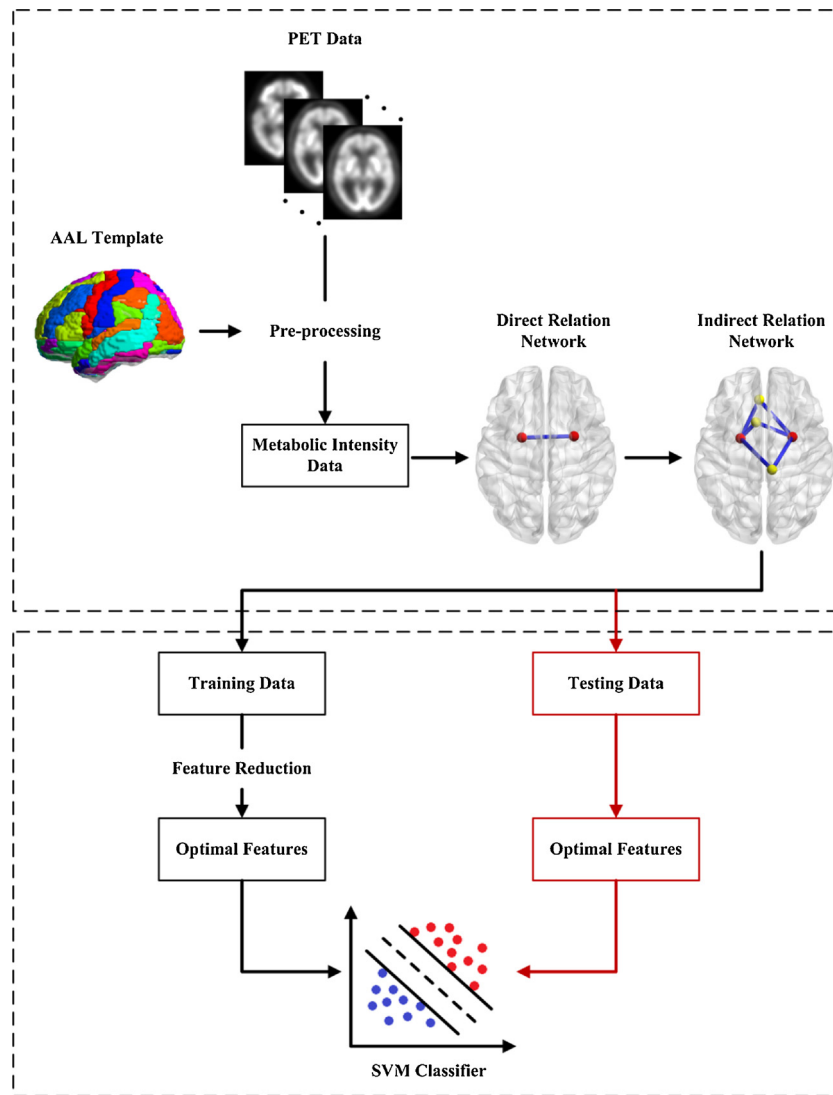


Fig. 1. The proposed classification framework.

full-width-at-halfmaximum (FWHM). In conclusion, images labeled with “Coreg, Avg, Std Img and Vox Siz, Uniform Resolution” were downloaded and used in this study.

2.2. Classification framework

The framework of our proposed indirect relation based individual network for classification is provided in Fig. 1. There are five main steps: 1) image pre-processing, 2) direct relation based network construction, 3) indirect relation based network construction, 4) feature reduction, and 5) classification.

2.2.1. Image pre-processing

The spatial preprocessing of PET images was implemented by Statistical Parametric Mapping software package 8 (SPM8) (<http://www.fil.ion.ucl.ac.uk/spm>). PET images acquired from the same participant were firstly realigned to the mean image in the series. Then, all images were co-registered into the Montreal Neurological Institute (MNI) space to correct individual differences in brain morphological parameters.

2.2.2. Direct relation based network construction

In this study, the individual metabolic network was constructed based on cerebral glucose metabolism measurements from PET data.

Prior to network construction, cerebral glucose metabolism data of all brain regions except the cerebellum was normalized to [0,1] using Min-Max normalization (Han and Kamber, 2006), the normalized data was partitioned into 90 regions of interest (ROIs) by Automated Anatomical Labeling (AAL) (Tzouriomazoyer et al., 2002) template, and then the 90 ROIs were utilized as nodes of the network. For each ROI, mean signal intensity and standard deviation were computed. Then a 90×90 correlation matrix was constructed with every element representing the correlation of average intensity between a pair of ROIs (Wee et al., 2013).

Specifically, the dissimilarity of average intensity of two regions is defined by Euclidean metric:

$$d(\mathbf{a}, \mathbf{b}) = (t(\mathbf{a}) - t(\mathbf{b}))^2 \quad (1)$$

where $t(a)$ and $t(b)$ denote mean glucose metabolism intensity of region a and region b , respectively. The correlation of two regions is defined by exponential function:

$$r(\mathbf{a}, \mathbf{b}) = \exp\left(\frac{-d(\mathbf{a}, \mathbf{b})}{2(\sigma_a + \sigma_b)}\right) \quad (2)$$

where σ_a and σ_b denote the standard deviation of glucose metabolism intensity of region a and region b , respectively. The standard deviation is employed to improve dissimilarity magnitude and individual diversity (Zheng et al., 2015).

Based on above analysis, each subject obtained a 90×90 correlation matrix which was symmetric with ones along its diagonal. The elements in the matrix reflect the direct relation between a pair of ROIs. Then we replaced ones with zeros in diagonal, which means region itself has no relation. Therefore, direct relation based brain metabolic network was constructed for each subject.

2.2.3. Indirect relation based network construction

Although region-to-region correlation can reflect the relation of two regions directly, it is a rough representation and relies on limited information of two regions. The correlation of regions' relation, which is called the indirect relation, could provide more information and reflect two regions' correlation exactly. For each pair of regions, the indirect relation is calculated by following steps. Firstly, the K nearest neighbors of each region are found using direct relation values. Note that K is a parameter set by experiments. Secondly, the same nearest neighbors of two regions are regarded as their common neighbors. It's remarkable that two regions may have no common neighbors because their K nearest neighbors' sets do not intersect. In this case, we regard the two regions have no indirect relation and free the calculation behind. Thirdly, the direct relations of two regions and their common neighbors are represented by two feature vectors, respectively. At last, the correlation of the two feature vectors is described by lattice-close-degree.

Take region a and region b as example, we first sorted the direct relation values of region a to other regions in descending order. The greater the value, the closer the relationship is. So the K ($K \in [1, 89]$) nearest neighbors of region a were found. The same operation was done to region b to find its K nearest neighbors. Then we found the common neighbors of region a and region b , which were represented as set $U = \{n_1, n_2, \dots, n_M\}$, $M \in [1, 88]$. The direct relations of region a and region b to common neighbors were represented by feature vectors $\tilde{A}(n) = \{r(a, n_1), r(a, n_2), \dots, r(a, n_M)\}$ and $\tilde{B}(n) = \{r(b, n_1), r(b, n_2), \dots, r(b, n_M)\}$, $M \in [1, 88]$, respectively. Above process is illustrated in Fig. 2. The correlation of feature vectors $\tilde{A}(n)$ and $\tilde{B}(n)$ was computed to represent the indirect relation of region a and region b . The lattice-close-degree of fuzzy sets (Xie and Liu, 2013) was used to describe the correlation of two feature vectors.

$$\tilde{A} \circ \tilde{B} = \bigvee_{n \in U} [\tilde{A}(n) \wedge \tilde{B}(n)] \quad (3)$$

$$\tilde{A} \odot \tilde{B} = \bigwedge_{n \in U} [\tilde{A}(n) \vee \tilde{B}(n)] \quad (4)$$

where $\tilde{A} \circ \tilde{B}$ is the inner product, $\tilde{A} \odot \tilde{B}$ is the outer product. When $\tilde{A} \circ \tilde{B}$ is larger and $\tilde{A} \odot \tilde{B}$ is smaller, the two fuzzy sets are closer. The lattice-close-degree can be defined as follows:

$$\sigma(\tilde{A}, \tilde{B}) = \frac{1}{2} [\tilde{A} \circ \tilde{B} + (1 - \tilde{A} \odot \tilde{B})] \quad (5)$$

Obviously, when $\sigma(\tilde{A}, \tilde{B})$ is larger, the correlation of two feature vectors is greater. Specifically, if two regions don't have common neighbors, the value of indirect relation is set to be zero. For each subject, we computed the lattice-close-degree for each pair of ROIs, and obtained a 90×90 symmetric matrix. The diagonal of the matrix are set to be zeros also means region itself has no indirect relation. The upper triangle of each matrix was extracted and concatenated to form a feature vector with a length of $90 \times (90-1) / 2 = 4005$.

2.2.4. Feature reduction

Feature reduction is used to remove redundant and noisy variables, a process which mitigates the curse-of-dimensionality and small- n -large- p effects (Mwangi et al., 2014). Feature reduction in our framework includes two steps: t -test based feature subset selection and PCA dimensionality reduction. At first, an unpaired two-sample t -test was applied to retain features that showed statistical differences. Specifically, the features with significant differences ($p < 0.05$, uncorrected) between two different groups were retained. However, the feature set selected by t -test was discriminative but not optimal for classification. The selected features were correlated and the number was still far more than that of the samples. To deal with that, principal component analysis (PCA) (Jolliffe, 2002; López et al., 2011) was applied to further reduce dimensionality. PCA convert the original features to a smaller number of uncorrelated features with largest amount of variance by a linear transformation. The original features are firstly normalized using zero-mean normalization. Then, Eigen decomposition of the covariance matrix from the standardized data is performed. The resulting eigenvectors are a new set of uncorrelated features, whose variances are represented by eigenvalues. Thirdly, eigenvalues are sorted in

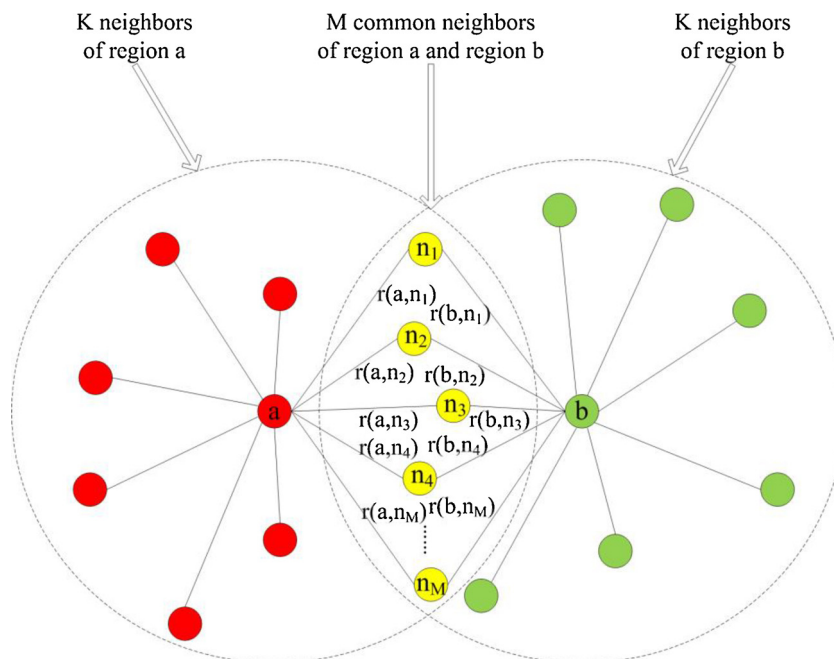


Fig. 2. The process of finding common neighbors of region a and region b .

decreasing order and the ‘leading’ eigenvectors explaining most of the variance in the data are found. Lastly, principal components are constructed by multiplying the originally normalized data with the ‘leading’ eigenvectors whose exact number is a user-defined parameter. In this study, PCA was applied to the selected feature set by *t*-test and fewer uncorrelated features were acquired for classification.

2.2.5. Classification

Based on the extracted features above, the classification model was constructed using support vector machine (SVM) (Cortes and Vapnik, 1995) classifier. The aim of SVM is to find the maximum margin hyperplane that represent the largest margin between two clinical groups in the feature space. The boundaries of the hyperplane were represented by support vectors, equivalent to the training samples on the margins. In this study, SVM with radial basis function (RBF) kernel was performed using LIBSVM (Chang and Lin, 2001) on MATLAB. The RBF kernel is formulated as follows:

$$k(x_i, x_j) = \exp\left(-\frac{\|x_i - x_j\|^2}{2\sigma^2}\right) \quad (6)$$

where x_i and x_j are two feature vectors, and σ is the width of the Gaussian kernel. To acquire an unbiased estimate of true classification performance, we employed 10-fold cross-validation that initially divided all samples to 10 subsets and then iteratively left one subset out of training for subsequent testing until each of the 10 subsets were validated. To avoid possible bias, we repeated the cross-validation process for 10 times and obtained a mean value of classification performance. The default parameters were used for SVM.

3. Results

3.1. Classification performance

The classification performance between direct relation features in (Wee et al., 2013) and the proposed indirect relation features were compared firstly in this subsection. Then, two relation features were integrated to identify whether the performance could be improved. In addition, Mini-Mental State Exam (MMSE) scores and Alzheimer’s Disease Assessment Scale-cognitive subscale (ADAS-cog) scores were considered to be important clinical variables to help evaluate the stage of AD pathology and predict future progression, providing outstanding contribution for accuracy improvement (Landau et al., 2011; Li et al., 2014; Chen et al., 2016; Liu et al., 2017). In this work, the indirect relation features and two clinical variables were combined respectively by concatenating into a vector for further improvement. The performance of each compared feature was evaluated by mean classification accuracy, sensitivity, specificity and area under receiver operating characteristic curve (AUC). In order to examine whether the difference in classification accuracy was statistically significant, a paired *t*-test at 95% significance level was conducted.

As is shown in Table 2, the performance of indirect relation features was significantly better than that of the direct relation features in two tasks. In particular, the accuracy was achieved to 83.29% in distinguishing MCI patients from healthy controls with AUC of 0.9254, sensitivity of 78.43% and specificity of 88.74%. The small *p*-value ($p < 0.0001$) for classification accuracy also indicated the superiority of the indirect relation features over the direct relation features. However, compared to indirect relation features, the integrated relation features didn’t exhibit better performance except specificity reached to 90.22%. When entered clinical variable, further significant improvement was observed in MCI/NC classification task. Particularly, the accuracy was achieved to 86.40% ($p < 0.0001$) with a high AUC of 0.9360, sensitivity of 79.55% and specificity of 95.02% when ADAS-cog scores entered, which indicated excellent diagnostic power of the combined features.

In the prediction of MCI-to-AD conversion, Table 2 shows our

proposed framework performed much better than that using direct relation features, which achieved the accuracy and AUC of 79.47% ($p < 0.0001$) and 0.8692. The integrated relation features had no significant differences with indirect relation features in accuracy, sensitivity and specificity by *t*-test ($H = 0$), but it achieved a higher AUC of 0.8731. The predictive power met an increasing promotion when combined indirect relation features with ADAS-cog scores, the final accuracy achieved to 83.59%, with sensitivity of 82.26%, specificity of 85.37% and AUC of 0.9255. Therefore, compared to MMSE scores, ADAS-cog scores provided more complementary information for indirect relation features.

Fig. 3 illustrates the receiver operating characteristic (ROC) curve of relation features, clinical variables, and combination of indirect relation features with clinical variables in two tasks. It can be clearly observed that the indirect relation features derived from direct relation features surpassed its original form. In addition, ADAS-cog scores and MMSE scores exhibited different distinguishing abilities, so indirect relation features combined with proper clinical variable can obtain encouraging results in classification and prediction.

3.2. Discriminative indirect relations

In this subsection, we found the discriminative indirect relations using *t*-test for above two tasks respectively. To remove the effect of age and gender, a linear regression was performed before statistical analysis. An unpaired two-sample *t*-test with threshold of 0.05 was applied to find the discriminative indirect relations. Then, the comparison was corrected using Benjamini and Hochberg’s false discovery rate (BH-FDR) control algorithm, which is to find the maximum i meets $p_i < i * 0.05/n$ ($n = 4005$) (Benjamini and Hochberg, 1995; Benjamini et al., 2006).

Fig. 4(a) shows the average indirect relation networks of NC and MCI (neighbor’s number $K = 7$), while Fig. 4(b) shows the average indirect relation networks of sMCI and pMCI (neighbor’s number $K = 24$). In each group, although two networks look similar, a few differences can be found (see the red circle). In NC/MCI group, some indirect relations between areas such as hippocampus and inferior occipital gyrus, middle temporal gyrus and inferior temporal gyrus, amygdala and angular gyrus, insula and inferior temporal gyrus are all observed increasing trend, while the indirect relations between areas such as bilateral hippocampus, caudate nucleus and thalamus, rolandic operculum and parahippocampal gyrus, insula and caudate nucleus shows decreasing trend.

In the third line of Fig. 4, significant differences exist in the indirect relations were marked as black in binary images. The significant difference proportion of indirect relation in pMCI vs. sMCI (26.17%) is lower than that in MCI vs. NC (30.31%), corresponding to the fact that the boundary of these two subgroups is hard to distinguish and also explaining that separating pMCI from sMCI is a challenging task. Top 20 discriminative indirect relations listed in Table 3 for separating pMCI from sMCI, were selected by *t*-test and BH-FDR correction. It can be observed that the discriminative indirect relations widely exist in the whole brain rather than only in the side of hemisphere. These abnormal changes are visualized in Fig. 5 and the abbreviations are listed in Table 4.

3.3. The most discriminative regions

In this subsection, the most discriminative regions were found using a weight-based statistics method for each task, respectively. Firstly, the top 200 discriminative indirect relations were selected by *t*-test ($p < 0.05$, BH-FDR corrected) and sorted in ascending order of *p* value. It was obvious that the brain regions involved in the indirect relations with smaller *p* value are more discriminative. Hence, the brain regions in different indirect relations should be set to different weights. The brain region’s weight in one relation was defined in equation (7). Then,

Table 2
Classification and prediction performance of different features.

Feature	MCI vs. NC				pMCI vs. sMCI			
	ACC (%)	SEN (%)	SPE (%)	AUC	ACC (%)	SEN (%)	SPE (%)	AUC
Relation feature								
Direct relation	76.09	77.94	73.96	0.8213	69.05	68.69	71.55	0.7569
Indirect relation	83.29	78.43	88.74	0.9254	79.47	76.49	83.20	0.8692
Direct relation + Indirect relation	82.79	76.54	90.22	0.9156	78.69	75.47	81.34	0.8731
Clinical variables								
MMSE score	70.39	77.70	64.08	0.7377	62.03	63.82	61.32	0.5398
ADAS-cog score	76.18	75.16	77.82	0.8359	74.60	83.06	66.11	0.7901
Relation feature + Clinical variables								
Indirect relation + MMSE score	82.15	74.07	92.13	0.9435	75.12	72.66	78.88	0.8658
Indirect relation + ADAS-cog score	86.40	79.55	95.02	0.9360	83.59	82.26	85.37	0.9255

ACC = accuracy; SEN = sensitivity; SPE = specificity; AUC = area under ROC curve.

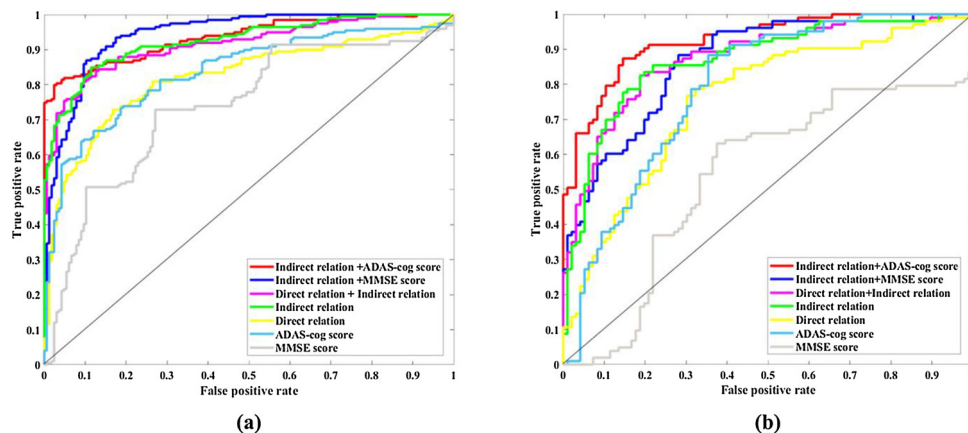


Fig. 3. (a) ROC curve of MCI vs. NC; (b) ROC curve of pMCI vs. sMCI (For interpretation of the references to colour in this figure legend, the reader is referred to the web version of this article).

for each region, the weights in the top 200 discriminative indirect relations were counted. After normalization, the weight of each brain region was obtained. Fig. 6 shows the results and 10 most discriminative regions are labeled by abbreviations (The abbreviations are also listed in Table 4). It could be observed that the regions: hippocampus, temporal pole: superior temporal gyrus, caudate nucleus, Lenticular nucleus, pallidum are four most discriminative regions in both MCI diagnosis and convert prediction, which means they changed significantly in different stages of neurodegenerative disease. The regions inferior temporal gyrus, angular gyrus, inferior occipital gyrus and insula also played an important role in MCI vs. NC classification. In separating pMCI from sMCI, the abnormal regions also include: amygdala, precentral gyrus, temporal pole: middle temporal gyrus, bilateral parahippocampal gyrus and cuneus.

$$w = -\lg(p) \quad (7)$$

4. Discussion

This study introduced a novel feature extraction method to establish individual network using FDG-PET data for the identification of mild cognitive impairment. Unlike computing region-to-region correlation only using limited between-region information, we proposed the indirect relation that is the correlation of regions' relation, which could provide deep inherent information for studying MCI. The lattice-close-degree in fuzzy mathematics was applied to reflect region-to-region indirect relation. Results suggest that our method outperformed direct relation features using a large number of subjects from ADNI database. Lastly, a weight-based statistics method was employed to find the most

discriminative regions involved in the discriminative indirect relations.

4.1. Classification performance analysis

The change of glucose metabolism caused by AD and MCI pathological attacks are not restricted to certain brain areas, but widely spread over the whole brain (Langbaum et al., 2009; Illan et al., 2011). Compared to ROI-based and voxel-based characteristics, the correlative features reveal the alterations between brain regions either adjacent or distant and might convey more useful information. In addition, the brain network is regarded to be relatively less sensitive to the influence of individual diversity and more robust than ROI-based characteristics (Dai et al., 2012; Zheng et al., 2015). Therefore, the network construction using between-region information has been successfully applied in classification and abnormal regions recognition. Based on further study, the indirect relation network we presented can reflect two regions' relation exactly in virtue of exploiting more regions' inherent information. In MCI diagnosis, results show that indirect relation alterations are more discriminative than direct relation alterations, and they give better classification performance (see Table 2). It is noteworthy that the high AUC of 0.9254 can reflect high precision and great power in MCI automatic diagnosis. However, when integrating two relation features, performance is not better than that of indirect relation features, suggesting two relation features have some redundant information owing to indirect relation derived from direct relation. To further promote classification performance, we combine the reduced indirect relation features with clinical variables. As shown in Table 2, ADAS-cog scores are more discriminative than MMSE scores. Therefore, significant improvements (accuracy of 86.40%) are achieved by combining indirect

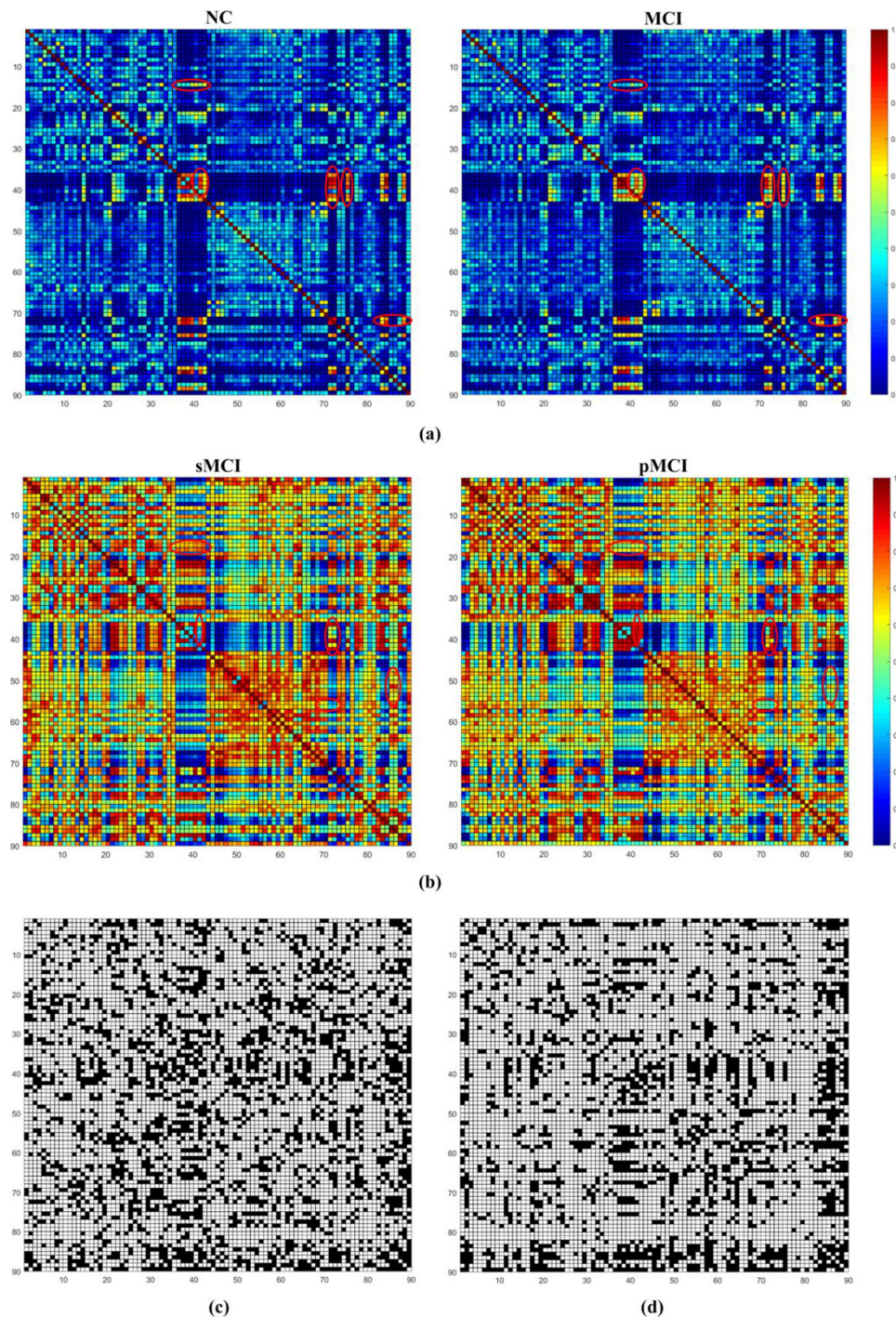


Fig. 4. (a) the average indirect networks of NC and MCI (neighbor's number $K = 7$); (b) the average indirect networks of sMCI and pMCI (neighbor's number $K = 24$). In each group, two networks look similar, but a few differences can be found (see the red circle). The third row shows the between-group differences of indirect relations ($p < 0.05$, BH-FDR corrected): (c) MCI vs. NC, (d) pMCI vs. sMCI. (For interpretation of the references to colour in this figure legend, the reader is referred to the web version of this article).

relation features with ADAS-cog scores, indicating excellent diagnostic power and generalizability of the combined features to unseen dataset. Note that the high specificity of 95.02% also indicates our method has extremely low false rate in MCI diagnose. In addition, the results imply that ADAS-cog scores deliver some complementary information into indirect relation features.

The identification of MCI converters from non-converters is critical for preventing or delaying AD, particularly from a clinical and financial perspective. Our findings demonstrate that the proposed framework can detect the subtle correlation changes of brain regions' glucose

metabolism that help to identify those MCI individuals who converted to AD up to 36 months before clinical diagnosis. As shown in Table 2, poor performance of MMSE scores denotes the fact pMCI and sMCI have less difference in this clinical variable. Yet when entered ADAS-cog scores, the predicted accuracy is reach to 83.59% with a high AUC value of 0.9255, which also due to ADAS-cog scores provide useful complementary information for indirect relation features.

Table 3
Top 20 discriminative indirect relations in pMCI vs. sMCI.

Rank	Indirect Relation	Rank	Indirect Relation
1	Precentral_L - Postcentral_L	11	Caudate_R - Temporal_Pole_Mid_R
2	Olfactory_L - Olfactory_R	12	ParaHippocampal_R - Amygdala_R
3	Frontal_Sup_R - Frontal_Mid_R	13	Precentral_L - Supp_Motor_Area_R
4	ParaHippocampal_R - Amygdala_L	14	Supp_Motor_Area_R - Paracentral_Lobule_R
5	Calcarine_L - Cuneus_L	15	Amygdala_L - Temporal_Pole_Sup_L
6	ParaHippocampal_L - Temporal_Pole_Sup_L	16	Temporal_Pole_Sup_L - Temporal_Pole_Sup_R
7	Temporal_Pole_Mid_L - Temporal_Pole_Mid_R	17	Precentral_L - Calcarine_L
8	Precentral_L - Cuneus_L	18	Hippocampus_L - Amygdala_L
9	ParaHippocampal_L - ParaHippocampal_R	19	Temporal_Pole_Sup_L - Temporal_Pole_Mid_R
10	Amygdala_L - Temporal_Pole_Mid_R	20	Cuneus_L - Cuneus_R

L = left; R = right.

4.2. Methods analysis

The indirect relation based individual network construction via glucose metabolism can be divided into direct relation calculation and indirect relation calculation. Direct relation calculation computes the correlation of two regions using Gaussian kernel function. The direct relation of two regions with their common neighbors constitute two fuzzy sets, the close-degree of two fuzzy sets, which represents indirect relation of two regions, is calculated by lattice-close-degree. The explanation of our network performed better may be as follows: 1) Using indirect relation of regions. In our study, the correlation of two regions is reflected by close-degree of multi-region rather than between-region information. Indirect relation employs abundant inherent information, which is robust to noise and individual diversity in glucose metabolism. 2) Two-step feature reduction method. In this work, a two-step feature reduction method includes two-sample *t*-test and PCA is used to find a feature subset for SVM classifier. Two-sample *t*-test, which is one of statistical hypothesis testing techniques, has extensively been used to detect group-level differences in neuroimaging studies (Saeyns et al., 2007; Mwangi et al., 2014). It is computationally fast and scale well to high dimensional data meaning it could select a small subset of relevant features from the original high-dimensional indirect relation features. However, although the features with no significant difference have been removed, the remaining features are still far more than the

Table 4
Abbreviations of the AAL regions shown in Fig.5 and Fig. 6.

Region ID	AAL regions	Abbreviations
1	Precentral	PreCG
2	Postcentral	PoCG
3	Olfactory	OLF
4	Frontal_Sup	SFGdor
5	Frontal_Mid	MFG
6	ParaHippocampal	PHG
7	Amygdala	AMYG
8	Calcarine	CAL
9	Cuneus	CUN
10	Temporal_Pole_Sup	TPOsup
11	Temporal_Pole_Mid	TPOmid
12	Caudate	CAU
13	Supp_Motor_Area	SMA
14	Paracentral_Lobule	PCL
15	Hippocampus	HIP
16	Pallidum	PAL
17	Temporal_Inf	ITG
18	Angular	ANG
19	Occipital_Inf	IOG
20	Insula	INS

samples. To overcome the overfitting problem, PCA is used to further reduce feature dimensionality. The relevant features with significant differences are transformed into a smaller number of uncorrelated variables by PCA, which are used for subsequent classification. Two-step feature reduction is also important for the integration of indirect features and clinical variable, because a large number of indirect relation features would weaken the role of clinical variable.

4.3. Discriminative regions analysis

We utilized *t*-test ($p < 0.05$, BH-FDR corrected) to find the discriminative indirect relations for each task. The discriminative indirect relations mentioned above are located either in the same hemisphere, or widely spread over the whole brain, suggesting the abnormalities caused by MCI have affected the entire brain rather than certain areas. Additionally, it is a remarkable fact that the indirect relation is more discriminative, the regions it involved are more likely to be abnormal alterations. Hence, we employed a weight-based statistics method which used *p*-value and logarithmic function to find the most discriminative abnormal regions. The brain regions we found (see Fig.6) have been reported to have abnormal alterations in MCI patients, as well as in AD conversion process, such as caudate nucleus, cuneus and precentral gyrus (Pagani et al., 2015), inferior occipital gyrus (Khazaei et al., 2016), hippocampus and amygdala (Pagani et al., 2015;

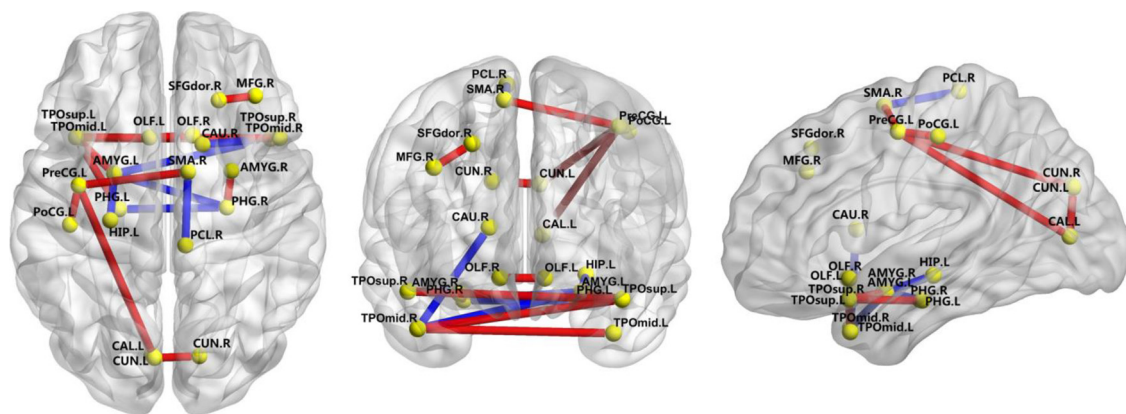


Fig. 5. Visualization of the top 20 discriminative indirect relations selected by *t*-test ($p < 0.05$, BH-FDR corrected). Red (blue) line means the average weight in pMCI group is larger (smaller) than that in sMCI group. (For interpretation of the references to colour in this figure legend, the reader is referred to the web version of this article).

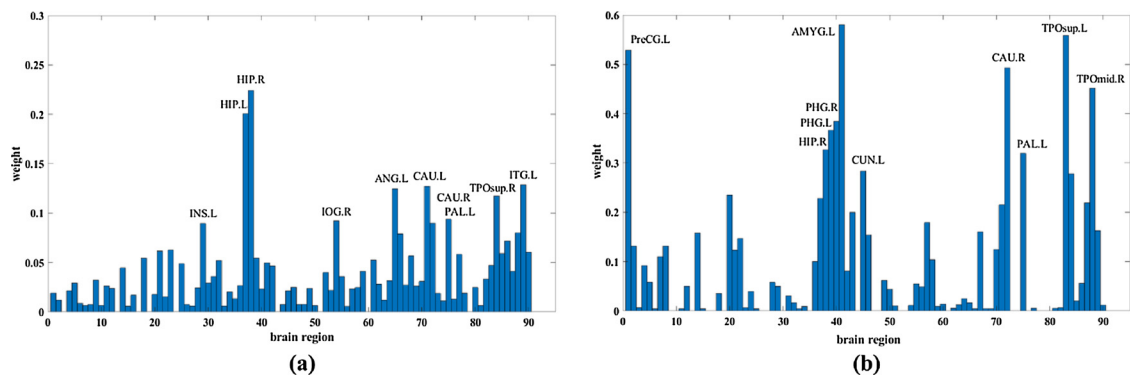


Fig. 6. Weights of brain regions in the top 200 discriminative indirect relations: (a) MCI vs. NC, (b) pMCI vs. sMCI. The most discriminative regions were labeled by abbreviations.

Youssofzadeh et al.,2017), lenticular nucleus, pallidum (Sanabriadiatz et al., 2013; Ballarini et al., 2016), parahippocampal gyrus (Reiman et al., 2001; Kim et al., 2005; Youssofzadeh et al.,2017), temporal pole: superior temporal gyrus (Chen et al., 2016), angular gyrus, inferior and middle temporal gyrus (Khazaei et al., 2016; Wang et al., 2016), insula (Chételat et al., 2008; Misra et al., 2009; Förster et al., 2010; Ewers et al., 2011). The fact that our findings are consistent with previous studies indicates the efficacy of our constructed network in identifying correct biomarkers for diagnosing MCI and predicting its conversion.

4.4. Limitations

Despite addressing some challenges, a number of limitations exist in the present study. Firstly, as an influence factor to the performance, the number of common neighbors K was set by experiments in this work. Hence, optimal method and more proper explanation should be exploited to set K . Secondly, another influence factor to classification accuracy is brain atlas (Ota et al., 2014; Min et al., 2015), other proper partition could be tried to improve the results. Future studies will apply the framework to other imaging data modalities, such as A β PET and MRI. Since the indirect relation based network of more imaging data modalities could describe the abnormal alterations in different perspectives. Besides, better close-degree description method of fuzzy sets also need to be explored.

5. Conclusions

In summary, we propose a novel approach of extracting individual network pattern from PET data. The network is constructed based on indirect relations, which could provide more inherent information and reflect regions' correlation exactly and overall. Moreover, a weight-based statistics method is employed to find the abnormal regions attacked by diseases. Results show that indirect relation features greatly exceed the performance of direct relation features in both classification and prediction. When combined with ADAS-cog scores, significant improvements can be observed. The most discriminative regions we found are consistent with previous studies indicate that our proposed network could identify correct biomarkers for MCI identification. In a word, this work offers a new network-based perspective for detecting MCI and predicting its conversion. Our results also give support to the feasibility of individual glucose metabolism network.

Conflict of interest

The authors declare that the research was conducted in the absence of any commercial or financial relationships that could be construed as a potential conflict of interest.

Ethics statements

The work described has been carried out in accordance with The Code of Ethics of the World Medical Association (Declaration of Helsinki) for experiments involving humans.

Acknowledgments

This work was supported by the National Basic Research Program of China (973 Program) (No. 2014CB744600), the National Natural Science Foundation of China (Grant No. 61632014, No. 61210010, No. 61572298), Program of Beijing Municipal Science & Technology Commission (No. Z171100000117005), Program of International S&T Cooperation of MOST (No. 2013DFA11140), the National Social Science Foundation of China (No. 16BGL181), the Natural Science Foundation of Shandong China (No. ZR201702130105) and A Project of Shandong Province Higher Educational Science and Technology Program (No. J17KB165). Data collection and sharing for this project was funded by the Alzheimer's Disease Neuroimaging Initiative (ADNI) (National Institutes of Health Grant U01 AG024904) and DOD ADNI (Department of Defense award number W81XWH-12-2-0012). ADNI is funded by the National Institute on Aging, the National Institute of Biomedical Imaging and Bioengineering, and through generous contributions from the following: AbbVie; Alzheimer's Association; Alzheimer's Drug Discovery Foundation; Araclon Biotech; BioClinica, Inc.; Biogen; Bristol-Myers Squibb Company; CereSpir, Inc.; Eisai Inc.; Elan Pharmaceuticals, Inc.; Eli Lilly and Company; EuroImmun; F. Hoffmann-La Roche Ltd and its affiliated company Genentech, Inc.; Fujirebio; GE Healthcare; IXICO Ltd.; Janssen Alzheimer Immunotherapy Research & Development, LLC.; Johnson & Johnson Pharmaceutical Research & Development LLC.; Lumosity; Lundbeck; Merck & Co., Inc.; Meso Scale Diagnostics, LLC.; NeuroRx Research; Neurotrack Technologies; Novartis Pharmaceuticals Corporation; Pfizer Inc.; Piramal Imaging; Servier; Takeda Pharmaceutical Company; and Transition Therapeutics. The Canadian Institutes of Health Research is providing funds to support ADNI clinical sites in Canada. Private sector contributions are facilitated by the Foundation for the National Institutes of Health (www.fnih.org). The grantee organization is the Northern California Institute for Research and Education, and the study is coordinated by the Alzheimer's Disease Cooperative Study at the University of California, San Diego. ADNI data are disseminated by the Laboratory for Neuro Imaging at the University of Southern California.

References

- Ballarini, T., Iaccarino, L., Magnani, G., Ayakta, N., Miller, B.L., Jagust, W.J., et al., 2016. Neuropsychiatric subsyndromes and brain metabolic network dysfunctions in early onset Alzheimer's disease. *Hum. Brain Mapp.* 37 (12), 4234–4247.
- Beheshti, I., Maikusa, N., Daneshmand, M., Matsuda, H., Demirel, H., Anbarjafari, G., 2017. Classification of Alzheimer's disease and prediction of mild cognitive

- impairment conversion using histogram-based analysis of patient-specific anatomical brain connectivity networks. *J. Alzheimers Dis.* 60 (1), 295–304.
- Benjamini, Y., Hochberg, Y., 1995. Controlling the false discovery rate: a practical and powerful approach to multiple testing. *J. R. Stat. Soc.* 57 (1), 289–300.
- Benjamini, Y., Krieger, A.M., Yekutieli, D., 2006. Adaptive linear step-up procedures that control the false discovery rate. *Biometrika* 93 (3), 491–507.
- Bischkopf, J., Busse, A., Angermeyer, M.C., 2002. Mild cognitive impairment—a review of prevalence, incidence and outcome according to current approaches. *Acta Psychiatr. Scand.* 106 (6), 403–414.
- Brookmeyer, R., Gray, S., Kawas, C., 1998. Projections of Alzheimer's disease in the United States and the public health impact of delaying disease onset. *Am. J. Public Health* 88 (9), 1337–1342.
- Camus, V., Payoux, P., Barré, L., Desgranges, B., Voisin, T., Tauber, C., et al., 2012. Using PET with 18F-AV-45 (florbetapir) to quantify brain amyloid load in a clinical environment. *Eur. J. Nucl. Med. Mol. Imaging* 39 (4), 621–631.
- Celone, K.A., Calhoun, V.D., Dickerson, B.C., Atri, A., Chua, E.F., Miller, S.L., et al., 2006. Alterations in memory networks in mild cognitive impairment and Alzheimer's disease: an independent component analysis. *J. Neurosci. Off. J. Soc. Neurosci.* 26 (40), 10222–10231.
- Chang, C.C., Lin, C.J., 2001. LIBSVM: a library for support vector machines. *ACM Trans. Intell. Syst. Technol. (TIST)* 2 (3), 1–27.
- Chen, G., Ward, B.D., Xie, C., Li, W., Wu, Z., Jones, J.L., et al., 2011. Classification of Alzheimer disease, mild cognitive impairment, and normal cognitive status with large-scale network analysis based on resting-state functional MR imaging. *Int. J. Med. Radiol.* 259 (1), 213–221.
- Chen, X., Yun, Z., Wang, R., Cao, H., Reid, S., Rui, G., et al., 2016. Potential clinical value of multiparametric PET in the prediction of Alzheimer's disease progression. *PLoS One* 11 (5), e0154406.
- Chételat, G., Desgranges, B., Landeau, B., Mézange, F., Poline, J.B., De, L.S.V., et al., 2008. Direct voxel-based comparison between grey matter hypometabolism and atrophy in Alzheimer's disease. *Brain* 131, 60–71.
- Cortes, C., Vapnik, V., 1995. Support-vector networks. *Mach. Learn.* 20 (3), 273–297.
- Dai, D., He, H., Vogelstein, J.T., Hou, Z., 2012. Accurate prediction of AD patients using cortical thickness networks. *Mach. Vis. Appl.* 24 (7), 1445–1457.
- Dartigues, J.F., 2009. Alzheimer's disease: a global challenge for the 21st century. *Lancet Neurol.* 8 (12), 1082–1083.
- Ewers, M., Sperling, R.A., Klunk, W.E., Weiner, M.W., Hampel, H., 2011. Neuroimaging markers for the prediction and early diagnosis of Alzheimer's disease dementia. *Trends Neurosci.* 34 (8), 430–442.
- Förster, S., Teipel, S., Zach, C., Rominger, A., Cumming, P., Cl, F., et al., 2010. FDG-PET mapping the brain substrates of visuo-constructive processing in Alzheimer's disease. *J. Psychiatr. Res.* 44 (7), 462–469.
- Frisoni, G.B., Fox, N.C., Jack Jr., C.R., Scheltens, P., Thompson, P.M., 2010. The clinical use of structural MRI in Alzheimer disease. *Nat. Rev. Neurol.* 6 (2), 67–77.
- Grundman, M., Petersen, R.C., Ferris, S.H., Thomas, R.G., Aisen, P.S., Bennett, D.A., et al., 2004. Mild cognitive impairment can be distinguished from Alzheimer disease and normal aging for clinical trials. *Arch. Neurol.* 61 (1), 59–66.
- Hafkemeijer, A., Möller, C., Dopfer, E.G., Jiskoot, L.C., Schouten, T.M., van Swieten, J.C., et al., 2015. Resting state functional connectivity differences between behavioral variant frontotemporal dementia and Alzheimer's disease. *Front. Hum. Neurosci.* 9, 474.
- Han, J., Kamber, M., 2006. *Data Mining: Concepts and Techniques*, second ed. Morgan Kaufmann, USA.
- Hänninen, T., Hallikainen, M., Tuomainen, S., Vanhanen, M., Soininen, H., 2000. Prevalence of mild cognitive impairment: a population-based study in elderly subjects. *Acta Neurol. Scand.* 21 (3), 148–154.
- He, Y., Chen, Z.J., Evans, A.C., 2007a. Small-world anatomical networks in the human brain revealed by cortical thickness from MRI. *Cereb. Cortex* 17 (10), 2407–2419.
- He, Y., Wang, L., Zang, Y., Tian, L., Zhang, X., Li, K., et al., 2007b. Regional coherence changes in the early stages of Alzheimer's disease: a combined structural and resting-state functional MRI study. *Neuroimage* 35 (2), 488–500.
- Hee-Jong, K., Jeong-Hyeon, S., Han, C.E., Jin, K.H., Na, D.L., Won, S.S., et al., 2016. Using individualized brain network for analyzing structural covariance of the cerebral cortex in Alzheimer's patients. *Front. Neurosci.* 10.
- Herholz, K., 2003. PET studies in dementia. *Ann Nucl. Med.* 17 (2), 79–89.
- Herholz, K., 2010. Cerebral glucose metabolism in preclinical and prodromal Alzheimer's disease. *Expert Rev. Neurother.* 10 (11), 1667–1673.
- Illan, I.A., Riz, J.M., Rez, J., Salas-Gonzalez, D., Pez, M.M., et al., 2011. 18F-FDG PET imaging analysis for computer aided Alzheimer's diagnosis. *Inf. Sci.* 181 (4), 903–916.
- Jie, B., Zhang, D., Gao, W., Wang, Q., Wee, C.Y., Shen, D., 2014a. Integration of network topological and connectivity properties for neuroimaging classification. *IEEE Trans. Biomed. Eng.* 61 (2), 576–589.
- Jie, B., Zhang, D., Wee, C.Y., Shen, D., 2014b. Topological graph kernel on multiple thresholded functional connectivity networks for mild cognitive impairment classification. *Hum. Brain Mapp.* 35 (7), 2876–2897.
- Jolliffe, I., 2002. *Principle Component Analysis*. Springer-Verlag, New York.
- Khazae, A., Ebrahimzadeh, A., Babajani-Feremi, A., 2016. Application of advanced machine learning methods on resting-state fMRI network for identification of mild cognitive impairment and Alzheimer's disease. *Brain Imaging Behav.* 10 (3), 799–817.
- Kim, E.J., Cho, S.S., Jeong, Y., Park, K.C., Kang, S.J., Kang, E., et al., 2005. Glucose metabolism in early onset versus late onset Alzheimer's disease: an SPM analysis of 120 patients. *Brain J. Neurol.* 128 (Pt 8), 1790–1801.
- Landau, S.M., Harvey, D., Madison, C.M., Koeppe, R.A., Reiman, E.M., Foster, N.L., et al., 2011. Associations between cognitive, functional, and FDG-PET measures of decline in AD and MCI. *Neurobiol. Aging* 32 (7), 1207–1218.
- Langbaum, J.B.S., Chen, K., Lee, W., Reschke, C., Dan, B., Fleisher, A.S., et al., 2009. Categorical and correlational analyses of baseline fluorodeoxyglucose positron emission tomography images from the Alzheimer's Disease Neuroimaging Initiative (ADNI). *Neuroimage* 45 (4), 1107–1116.
- Li, Y., Wang, Y., Wu, G., Shi, F., Zhou, L., Lin, W., et al., 2012. Discriminant analysis of longitudinal cortical thickness changes in Alzheimer's disease using dynamic and network features. *Neurobiol. Aging* 33 (2), 427 e15–427.e30.
- Li, M., Oishi, K., He, X., Qin, Y., Gao, F., Mori, S., 2014. An efficient approach for differentiating Alzheimer's disease from normal elderly based on multicenter MRI using gray-level invariant features. *PLoS One* 9 (8), e105563.
- Liu, K., Chen, K., Yao, L., Guo, X., 2017. Prediction of mild cognitive impairment conversion using a combination of independent component analysis and the cox model. *Front. Hum. Neurosci.* 11, 33.
- López, M., Ramírez, J., Górriz, J.M., et al., 2011. Principal component analysis-based techniques and supervised classification schemes for the early detection of Alzheimer's disease. *Neurocomputing* 74 (8), 1260–1271.
- Mayeux, R., Stern, Y., 2012. Epidemiology of Alzheimer disease. *Cold Spring Harb. Perspect. Med.* 2 (8), 137–152.
- Min, R., Wu, G., Cheng, J., Wang, Q., Shen, D., 2015. Multi-atlas based representations for Alzheimer's disease diagnosis. *Hum. Brain Mapp.* 35 (10), 5052–5070.
- Misra, C., Fan, Y., Davatzikos, C., 2009. Baseline and longitudinal patterns of brain atrophy in MCI patients, and their use in prediction of short-term conversion to AD: results from ADNI. *Neuroimage* 44 (4), 1415–1422.
- Mwangi, B., Tian, T.S., Soares, J.C., 2014. A review of feature reduction techniques in neuroimaging. *Neuroinformatics* 12 (2), 229–244.
- Nordberg, A., Rinne, J.O., Kadir, A., Långström, B., 2010. The use of PET in Alzheimer disease. *Nat. Rev. Neurol.* 6 (2), 78–87.
- Ota, K., Oishi, N., Ito, K., Fukuyama, H., S-S, Group, 2014. A comparison of three brain atlases for MCI prediction. *J. Neurosci. Methods* 221 (2), 139–150.
- Pagani, M., De, C.F., Morbelli, S., Öberg, J., Chincari, A., Frisoni, G.B., et al., 2015. Volume of interest-based [¹⁸F]fluorodeoxyglucose PET discriminates MCI converting to Alzheimer's disease from healthy controls. A European Alzheimer's disease consortium (EADC) study. *Neuroimage Clin.* 7, 34–42.
- Park, H.J., Friston, K., 2013. Structural and functional brain networks: from connections to cognition. *Science* 342 (6158), 1238411–1–8.
- Petersen, R.C., 2004. Mild cognitive impairment as a diagnostic entity. *J. Intern. Med.* 256 (3), 183–194.
- Prasad, G., Joshi, S.H., Nir, T.M., Toga, A.W., Thompson, P.M., 2015. Brain connectivity and novel network measures for Alzheimer's disease classification. *Neurobiol. Aging* 36 (3), S121–S131.
- Prince, M., Wimo, A., Guerchet, M., Ali, G.C., Wu, Y.T., Prina, M., 2015. *World Alzheimer Report 2015: The Global Impact of Dementia: An Analysis of Prevalence, Incidence, Cost and Trends*. Alzheimer's Disease International, London.
- Raj, A., Mueller, S.G., Young, K., Laxer, K.D., Weiner, M., 2010. Network-level analysis of cortical thickness of the epileptic brain. *Neuroimage* 52 (4), 1302–1313.
- Rathore, S., Habes, M., Iftikhar, M.A., Shacklett, A., Davatzikos, C., 2017. A review on neuroimaging-based classification studies and associated feature extraction methods for Alzheimer's disease and its prodromal stages. *Neuroimage* 155, 530–548.
- Reiman, E.M., Caselli, R.J., Chen, K., Alexander, G.E., Bandy, D., Frost, J., 2001. Declining brain activity in cognitively normal Apolipoprotein E ε4 heterozygotes: a foundation for using positron emission tomography to efficiently test treatments to prevent Alzheimer's disease. *Proc. Natl. Acad. Sci. U. S. A.* 98 (6), 3334–3339.
- Reisberg, B., Ferris, S.H., de Leon, M.J., Crook, T., 1982. The global deterioration scale for assessment of primary degenerative dementia. *Am. J. Psychiatry* 139 (9), 1136–1139.
- Saeys, Y., Inza, I., Larrañaga, P., 2007. A review of feature selection techniques in bioinformatics. *Bioinformatics* 23 (19), 2507–2517.
- Sanabria-diaz, G., Martínezmontes, E., Meliegarcía, L., 2013. Glucose metabolism during resting state reveals abnormal brain networks organization in the Alzheimer's disease and mild cognitive impairment. *PLoS One* 8 (7), e68860–e68860.
- Shao, J., Myers, N., Yang, Q., Feng, J., Plant, C., 2012. Prediction of Alzheimer's disease using individual structural connectivity networks. *Neurobiol. Aging* 33 (12), 2756–2765.
- Smith, M.A., Richey-Harris, P.L., Sayre, L.M., Beckman, J.S., Perry, G., 1997. Widespread peroxynitrite-mediated damage in Alzheimer's disease. *J. Neurosci. Off. J. Soc. Neurosci.* 17 (8), 2653–2657.
- Stam, C.J., Jones, B.F., Manhanden, I., Am, V.C.V.W., Montez, T., Verbunt, J.P., et al., 2006. Magnetoencephalographic evaluation of resting-state functional connectivity in Alzheimer's disease. *Neuroimage* 32 (3), 1335–1344.
- Tzouriomazoyer, N., Landeau, B., Papathanassiou, D., Crivello, F., Etard, O., Delcroix, N., et al., 2002. Automated anatomical labeling of activations in SPM using a macroscopic anatomical parcellation of the MNI MRI single-subject brain. *Neuroimage* 15 (1), 273–289.
- Wang, J., Wang, X., He, Y., Yu, X., Wang, H., He, Y., 2015. Apolipoprotein ε4 modulates functional brain connectome in Alzheimer's disease. *Hum. Brain Mapp.* 36 (5), 1828–1846.
- Wang, P., Chen, K., Yao, L., Hu, B., Wu, X., Zhang, J., et al., 2016. Multimodal classification of mild cognitive impairment based on partial least squares. *J. Alzheimers Dis.* 54 (1), 359–371.
- Wee, C.Y., Yap, P.T., Li, W., Denny, K., Browndyke, J.N., Potter, G.G., et al., 2011. Enriched white-matter connectivity networks for accurate identification of MCI patients. *Neuroimage* 54 (3), 1812–1822.
- Wee, C.Y., Yap, P.T., Shen, D., 2013. Prediction of Alzheimer's disease and mild cognitive impairment using cortical morphological patterns. *Hum. Brain Mapp.* 34 (12), 3411–3425.
- Xie, J., Liu, C., 2013. *Fuzzy Mathematical Method and Its Application* (in Chinese), fourth

- ed. Huazhong University of Science and Technology Press, China.
- Yao, Z., Hu, B., Zheng, J., Zheng, W., Chen, X., Gao, X., et al., 2015. A FDG-PET study of metabolic networks in Apolipoprotein E ϵ 4 allele carriers. *PLoS One* 10 (7), e0132300.
- Yao, Z., Hu, B., Nan, H., Zheng, W., Xie, Y., 2017. Individual metabolic network for the accurate detection of Alzheimer's disease based on FDGPET imaging. *IEEE International Conference on Bioinformatics and Biomedicine. IEEE*, 2017. pp. 1328–1335.
- Youssofzadeh, V., Mcguinness, B., Maguire, L.P., Wonglin, K.F., 2017. Multi-kernel learning with Dartel improves combined MRI-PET classification of Alzheimer's disease in AIBL data: group and individual analyses. *Front. Hum. Neurosci.* 11, 380.
- Yu, G., Liu, Y., Shen, D., 2015. Graph-guided joint prediction of class label and clinical scores for the Alzheimer's disease. *Brain Struct. Funct.* 221 (7), 1–15.
- Zheng, W., Yao, Z., Hu, B., Gao, X., Cai, H., Moore, P., 2015. Novel cortical thickness pattern for accurate detection of Alzheimer's disease. *J. Alzheimers Dis.* 48 (4), 995–1008.
- Zhou, L., Wang, Y., Yang, L., Yap, P.T., Shen, D., 2011. Hierarchical anatomical brain networks for MCI prediction: revisiting volumetric measures. *PLoS One* 6 (7), e21935.